Available online at www.sciencedirect.com

SCIENCE DIRECT®

Thin Solid Films 493 (2005) 307 – 312

thin solid films

www.elsevier.com/locate/tsf

Metastable phase evolution and grain growth in annealed nanocrystalline Cr–Fe–Ni films

E.D. Specht [a,*], P.D. Rack [b], A. Rar [a,b], G.M. Pharr [a,b], E.P. George [a,b], J.D. Fowlkes [b], H. Hong [c], E. Karapetrova [c]

[a] *Metals and Ceramics Division, Oak Ridge National Laboratory, Oak Ridge, Tennessee, 37831-6118, USA*
[b] *Department of Materials Science and Engineering, University of Tennessee, Knoxville, Tennessee, 37996, USA*
[c] *Frederick Seitz Materials Research Laboratory, University of Illinois at Urbana-Champaign, Urbana, Illinois, 61801, USA*

Received 6 October 2004; received in revised form 4 May 2005; accepted 20 July 2005
Available online 18 August 2005

Abstract

Nanocrystalline Cr–Fe–Ni thin films libraries are prepared by radio frequency magnetron sputter codeposition on Al_2O_3 substrates. The variation in distance from different points on the substrate to the three sputter sources produces a spread in composition in the films. Synchrotron radiation is used to analyze composition, crystallographic phase, and grain size as a function of sample position, both as-deposited and after annealing. In addition to three equilibrium phases (bcc, fcc and σ-FeCr), a fourth phase is observed which does not correspond to any equilibrium phase in the Cr–Fe–Ni system, but which is consistent with the α-Mn structure. The films are initially nanocrystalline; both equilibrium and nonequilibrium phases are observed. Ternary phase diagrams measured at annealing temperatures of 200–800 °C show that the stability of nanocrystalline material against thermal grain growth varies widely with composition, and that the crystallographic phase can be selected to be an appropriate heat treatment. Thus, the approach used here is useful for technologies such as magnetic recording media where understanding the stability of the nanograin structure is critical.
© 2005 Elsevier B.V. All rights reserved.

PACS: 68.60.Dv; 68.66.Nq; 81.05.Ys
Keywords: Cr–Fe–Ni; Sputtering; X-ray diffraction; Phase diagram

1. Introduction

Nanocrystalline materials promise to provide a variety of improved properties. High-permeability nanocrystalline Fe–Ni and Cr–Fe–Ni alloys are of particular interest for reducing wear in magnetic recording heads [1,2]. Nanocrystalline Cr–Fe–Ni alloys are potentially of more general interest as structural materials because they form the basis of stainless steels [3]. Here, we focus on nanocrystalline Cr–Fe–Ni alloys made by the combinatorial thin film synthesis technique.

An important issue in the application of nanocrystalline materials is grain growth. Because properties are strongly dependent on grain size, thermal treatment can be used to tailor properties, but the temperature at which materials can be processed and used is limited, since grain growth can quickly convert a nanocrystalline to a microcrystalline structure. Careful studies have been made of the thermal stability of Fe–Ni alloys, but only at a few compositions: we are aware of reports only for Ni, $Fe_{21}Ni_{79}$, $Fe_{33}Ni_{67}$, and $Fe_{50}Ni_{50}$ [3–5], and of no data at all for ternary Cr–Fe–Ni alloys.

Another issue that must be considered in the growth and thermal treatment of nanocrystalline materials is phase stability. Three equilibrium phases are recognized in the Cr–Fe–Ni ternary system: the α or bcc structure found in Cr and low temperature Fe, the γ or fcc structure found in Ni and high-temperature Fe, and the intermetallic σ-FeCr structure [6]. A metastable structure has been reported in $Cr_{17.5}Fe_{82.5}$ films grown by ion-assisted cosputter deposition. The structure is isomorphic to the α-Mn structure

* Corresponding author. Tel.: +1 865 574 7682.
E-mail address: spechted@ornl.gov (E.D. Specht).

0040-6090/$ - see front matter © 2005 Elsevier B.V. All rights reserved.
doi:10.1016/j.tsf.2005.07.285

(Pearson group cI58), a distorted bcc structure with 58 atoms per unit cell [7,8]. The fcc phase field in the Fe–Ni binary is expanded in nanocrystalline alloys [9]. We are not aware of any report that shows how thermal treatment of nanocrystalline material affects the phase boundaries of binary or ternary alloys in the Cr–Fe–Ni system.

To determine the extent to which Cr–Fe–Ni nanocrystalline alloys can be processed and used at elevated temperatures, combinatorial libraries were deposited, annealed, and characterized using synchrotron X-ray diffraction to determine the grain size and phase distribution. Films are grown using the composition–spread method by simultaneously depositing from Cr, Fe, and Ni sputter sources confocally arranged toward the receiving substrate; the film's composition varies continuously along the sample with the relative distance to the sources. A limitation of this technique is that the composition range cannot include the pure elements or binary alloys; we choose a range which includes the bcc, fcc, σ-FeCr, and α-Mn phases. For most compositions, the material grows with a grain size between 5 and 15 nm. Preliminary reports have been made of the metastablity of the α-Mn phase and of the hardness of these samples [10,11], but this paper is the first to examine the behavior systematically and report grain growth as a function of composition and annealing conditions.

2. Experimental details

Thin alloy films are grown on polished circular Al_2O_3 (sapphire) substrates, 102 mm in diameter with a $(1\bar{1}02)$ orientation. We avoid using $Al_2O_3(0001)$, which leads to a severe preferred orientation in the film [12], and Si substrates which lead to delamination on annealing [10]. Films are deposited onto fixed substrates using simultaneous RF magnetron sputtering from 51 mm diameter Cr, Fe, and Ni sources. The sputtering geometry is shown in Fig. 1. Each source is surrounded by a 51 mm tall cylindrical shield to minimize cross-contamination. Target centers are 16.5 cm from the substrate center and are tilted at 32° relative to the substrate normal. The Fe and Ni sources are 180° apart, with the Cr source 90° from both the Fe and the Ni.

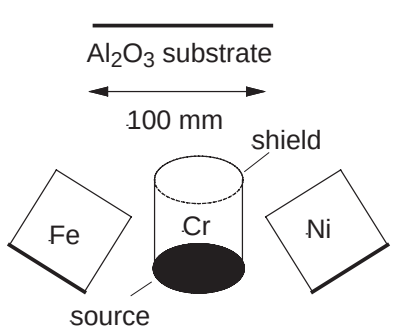

Fig. 1. 3-source sputter deposition system.

The chamber base pressure is 9×10^{-5} Pa and the deposition pressure is 1.3 Pa Ar. While the sputtering conditions (such as temperature, pressure, and deposition rate) can have a significant effect on the as-deposited film properties, the goal of this study is to investigate the phase evolution of the Cr–Fe–Ni films as a function of annealing temperature. Consequently, a sputtering pressure is used that yields an optimum deposition rate for this system. The sputtering powers are 160 W for Fe and 60 W for Cr and Ni. Deposition time is 3 h, yielding a film thickness of ~2 μm. Incidental heating from the sources raises the sample temperature to ~100 °C during deposition. After deposition, the samples are annealed without breaking vacuum at 200, 400, 600 and 800 °C, each for 2 h. An as-deposited sample is also studied.

The composition and structure are measured simultaneously by X-ray fluorescence and diffraction using synchrotron radiation at beamline X33-BM at the Advanced Photon Source. A double-crystal Si(111) monochromator selects 12 keV bending magnet X rays, which are sagitally focused by the monochromator and meridionally focused by a pair of mirrors, which also provide harmonic rejection. The focused beam size of 1.0×0.25 mm^2 creates a 1.0×1.0 mm^2 footprint on the sample when incident at a 15° glancing angle. The sample is rastered in a square grid in 2 mm steps. Data is collected for 2 s at each point.

Fluorescence spectra are acquired with a Si drift detector (165 eV resolution at 6.4 keV). The detector views the sample at a 15° glancing angle. The integrated counts in the Cr, Fe, and Ni K emission lines are measured by least-squares fitting to Gaussian lineshapes. The composition at each point is calculated from the ratio of these intensities using a method described previously [12]. Because the sample thickness is not constant, the thick-film limit is used in calculating the composition. This introduces a negligible error since incident X rays strike the sample at a glancing angle and the fluorescence X rays which are measured are emitted at the same glancing angle.

Diffraction patterns are collected with a 1024×1024 charge-coupled device detector. Instrumental resolution is determined by the broadening of diffraction rings produced by the beam size; increasing the distance from sample to detector improves resolution, at the price of observing a smaller range of 2θ and a smaller section of each diffraction ring. Diffraction patterns are integrated to give 2θ scans, from which phases are identified as described previously [12]. Assignment of diffraction peaks is illustrated in Fig. 2. Peak width is measured by least-squares fitting to Pearson-7 lineshapes. Peak breadth beyond instrumental resolution is generally caused by two factors. Microstrain, a distribution Δd of plane spacings d, produces breadth $\Delta 2\theta = 2\tan\theta\, \Delta d/d$. Particle size L produces breadth $\Delta 2\theta = 0.94\lambda/(L\cos\theta)$ [10]. Due to the effects of texture, overlapping peaks, and the low scattering intensity from nanocrystalline materials, it is not possible to comprehensively determine the nature of the observed peak broadening, but the as-deposited fcc phase

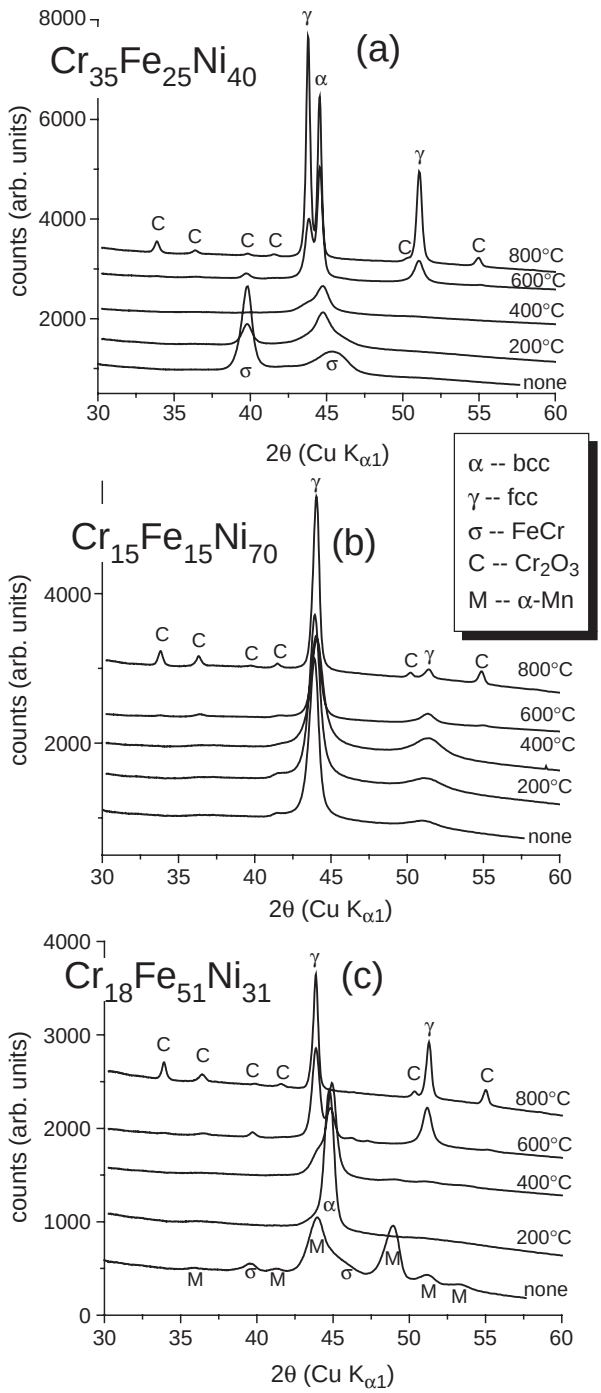

Fig. 2. Characteristic 2θ scans for samples annealed for 2 h at indicated temperatures; "none" indicates the as-deposited film. Intensities are offset for clarity. 2θ values have been converted to the equivalent values for Cu Kα1 radiation for convenience.

gives clear (111) and (200) reflections. The ratio of the widths of these reflections is consistent with grain-size broadening, indicating that grain size rather than strain makes the dominant contribution to peak width [10]. The average grain size at each composition is determined from the Scherrer equation [13]. Because the films grow with a strong preferred orientation, only one peak of each phase could be used in the grain size analysis: bcc(110), fcc(111), σ-FeCr(002), and α-Mn(332). Instrumental resolution was measured using a microcrystalline W sample and was subtracted from the peak widths. Grain sizes greater than ~30 nm cannot be reliably measured due to limited instrumental resolution.

3. Results

Qualitative trends can be seen in 2θ scans for three characteristic compositions annealed at four temperatures, shown in Fig. 2. Peaks are broadened for the as-deposited samples, and sharpen on annealing. A dramatic phase evolution occurs: a single-phase σ-FeCr film [$Cr_{35}Fe_{25}Ni_{40}$, Fig. 2(a)] converts to bcc at 200 °C, and to mainly fcc at 800 °C, while a single phase fcc film [$Cr_{15}Fe_{15}Ni_{70}$, Fig. 2(b)] remains so, and a mainly α-Mn film [$Cr_{18}Fe_{51}Ni_{31}$, Fig. 2(c)] converts to bcc at 200 °C and fcc at 600 °C. Cr_2O_3 peaks are visible at 600 and 800 °C; this is most likely a result of residual gas in the annealing vacuum [11].

Ternary plots of grain size evolution are given in Figs. 3–6. The lighter black lines in each plot denote the edge of the film, spanning a roughly triangular region of the ternary section. A limitation of the ternary codeposition technique is that the film cannot include pure elements or binary compositions. Each sample spans a slightly different composition due to temporal variations in sputter source output. The σ-FeCr structure occurs over a wide range of compositions in the as-deposited film (Fig. 3). Annealing at

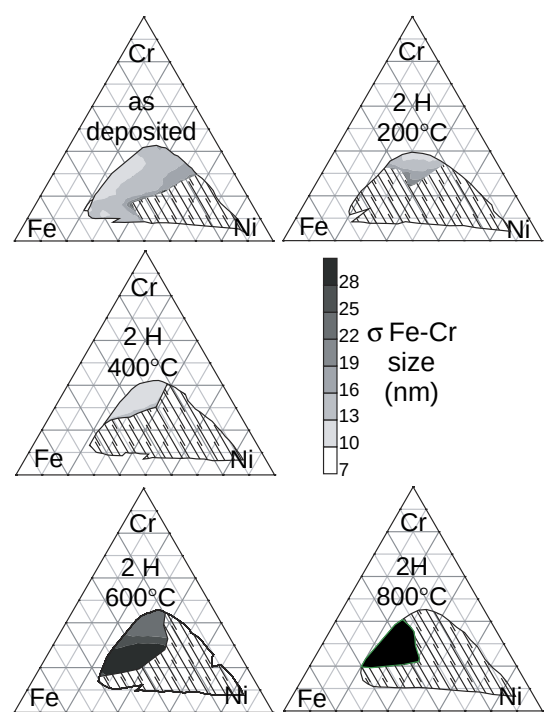

Fig. 3. Grain size and phase fields for σ-FeCr structure. Hatch indicates compositions where the σ-FeCr phase is not observed.

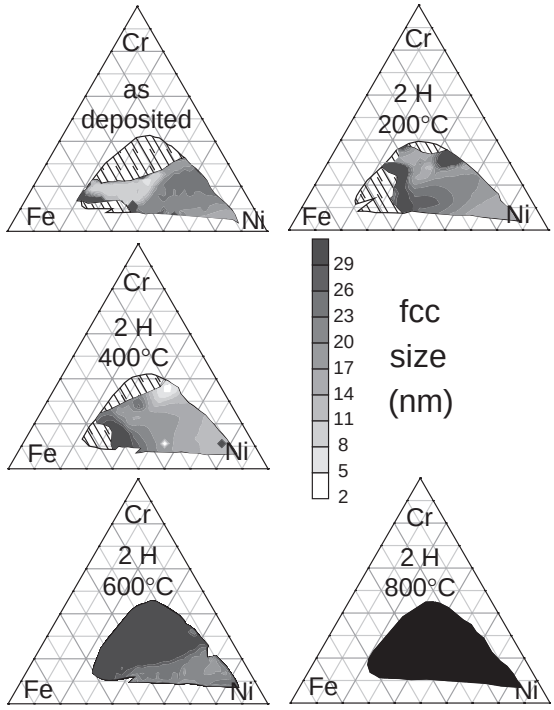

Fig. 4. Grain size and phase fields for fcc structure. Hatch indicates compositions where the fcc phase is not observed.

even the lowest temperature (200 °C) contracts the phase field greatly, perhaps because σ-FeCr is metastable at low temperatures. The as-deposited grain size of 10 to 13 nm does not increase significantly until 600 °C, where significant grain growth (>30 nm) occurs.

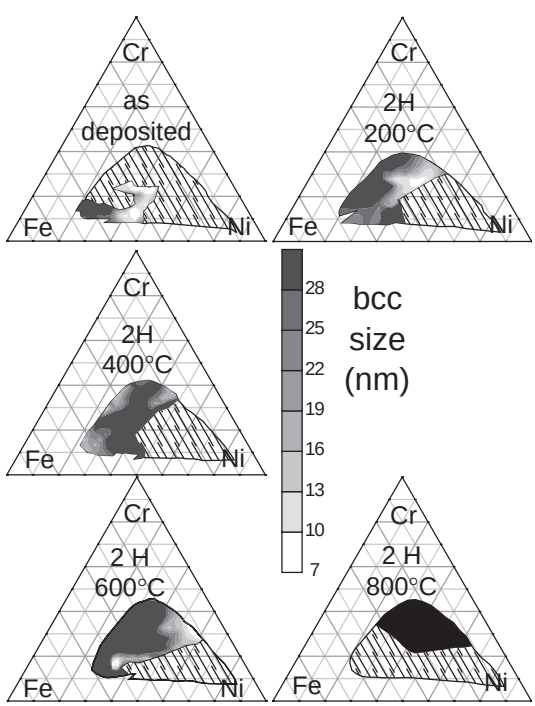

Fig. 5. Grain size and phase fields for bcc structure. Hatch indicates compositions where the bcc phase is not observed.

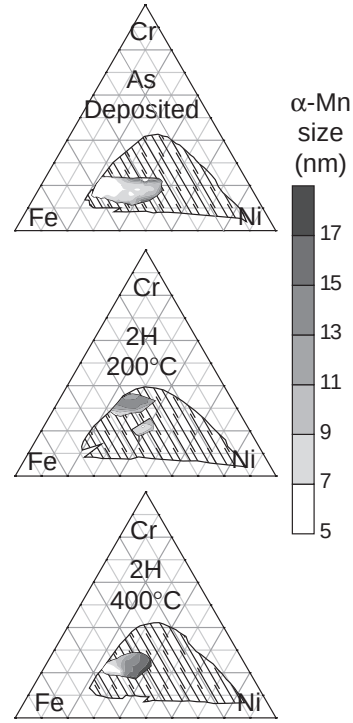

Fig. 6. Grain size and phase fields for α-Mn structure. While observable at 200 and 400 °C, the α-Mn peaks are very weak. Hatch indicates compositions where the α-Mn phase is not observed.

The fcc structure, on the other hand, spans a phase field less than its equilibrium extent below 600 °C; at this temperature and above it spans the entire film (Fig. 4). The as-deposited fcc-structure film has a grain size which depends strongly on composition: 5 nm nanocrystalline crystallites occur in the Fe-rich region where fcc, bcc, and σ-Fe structures coexist, while 20 nm crystallites form in the Ni-rich, single phase fcc field. As for σ-FeCr, significant grain growth occurs at 600 °C.

The bcc structure appears largely as a transitional phase (Fig. 5). It occurs over a narrow compositional range in the as-deposited film, it is found over a much wider range at intermediate temperatures (200–600 °C) as σ-FeCr transforms to bcc, and becomes again less widespread at the highest temperature (800 °C) as bcc transforms to fcc. The as-deposited grain size distribution is again bimodal, with 12 nm crystallites in the four-phase coexistence field and larger crystallites in the Fe-rich bcc + σ-FeCr field.

The α-Mn structure occurs in significant quantity only in the as-deposited sample (Fig. 6). The structure is barely detectable in the annealed samples [Fig. 2(c)], so the significance of the phase field and grain size in the sample is uncertain. The grain size is 5–10 nm as-grown (Fig. 6).

4. Discussion

Simmonds et al. reported the formation of the α-Mn structure in $Cr_{17.5}Fe_{82.5}$ grown by ion-assisted cosputter

deposition; without the ion assistance, the film grows with the bcc structure [8]. We find that compositions surrounding $Cr_{17}Fe_{49}Ni_{34}$ grow in a mixture of the α-Mn, fcc, and σ-FeCr structures, with no ion assist. This suggests that the ternary compounds form the metastable α-Mn structure more readily. Alternatively, if Simmonds et al. are correct in concluding that growth stress stabilizes α-Mn, its increased stability may be due to decreased stress relaxation in nanocrystalline mixtures, caused by an increase in strength with decreasing grain size. The yield strength of materials generally varies as the inverse square root of grain size. While strength may saturate or even decrease for grain sizes below the ~10 nm observed for as-deposited α-Mn, this small grain size is associated with high strength in a variety of metals [14].

As the samples are annealed at progressively higher temperatures, the phase content evolves from largely σ-FeCr as-deposited, to more bcc, and finally to mainly fcc. The phase fields at 800 °C are consistent with the equilibrium values calculated by Rar et al. [11] (Fig. 7) — differences of <5% may be caused by the formation of Cr_2O_3, which leads to a difference between the composition measured by X-ray fluorescence and the actual composition of the metal. The samples annealed at lower temperatures are clearly out of equilibrium. The as-deposited, 200 and 400 °C samples contain four-phase fields, in violation of the Gibbs phase rule [15]. The phase field for the 600 °C sample are far from the equilibrium values (Fig. 7). The time and temperature required for equilibration–2 h at 800 °C–is consistent with reports of Rar et al. on the thermal equilibration of Cr–Fe–Ni films [11].

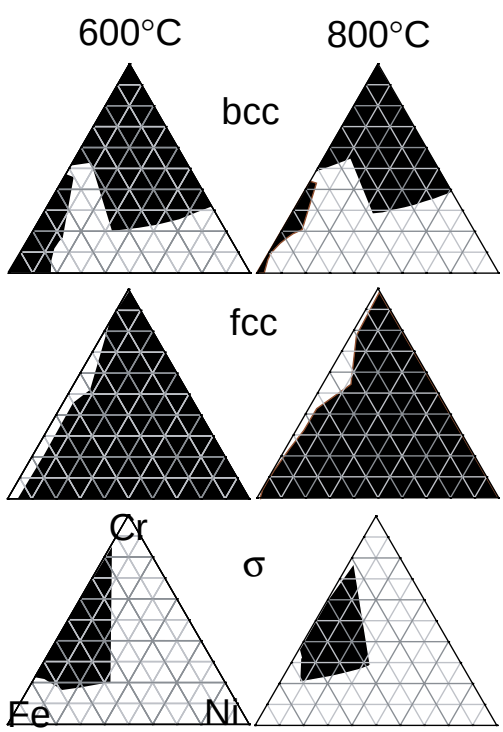

Fig. 7. Equilibrium phase fields calculated from thermodynamic data [11].

In the as-deposited films, nanocrystalline material occurs in the multiphase mixtures; grain growth occurs more readily in single-phase compositions. Our results for ternary compounds are consistent with those of Wang et al. for Fe–Ni binaries: in mixed-phase material, the bcc phase has a smaller grain size than the fcc phase [9].

Cheung et al. report a trend in electrodeposited fcc nanocrystalline Fe–Ni films: the as-deposited grain size decreases from 21 nm in pure Ni to 11 nm in $Fe_{28}Ni_{72}$ [2]. We observe the opposite trend in cosputtered films: the as-deposited fcc grain size increases from 14 nm in $Cr_6Fe_8Ni_{85}$ to 23 nm in $Cr_{10}Fe_{32}Ni_{58}$. It is unclear whether the reversal of this trend is due to the presence of Cr or to the different film growth techniques.

Thuvander et al. report that nanocrystalline fcc $Fe_{67}Ni_{33}$ forms microcrystalline grains when aged at room temperature, while $Fe_{50}Ni_{50}$ exhibits rapid grain growth only at temperatures of 400 °C and above [4]. We find that this trend holds in ternary Cr–Fe–Ni alloys. The fcc phase of Fe-rich alloys forms large grains at 200 °C, while nanocrystalline material growth appears in progressively more Ni-rich compositions at 600 and 800 °C. The addition of Cr restricts grain growth to higher temperatures.

Li and Ebrahimi find that significant grain growth in nanocrystalline fcc $Fe_{21}Ni_{79}$ occurs at temperatures of 600 to 700 °C [3]. We observe the same behavior in Cr–Fe–Ni ternaries with nearly the same composition; average grain size remains at 8 nm up to 400 °C, grows to 15 nm at 600 °C, and is >30 nm at 800 °C.

More detailed study will be required to measure the rate and activation energy of grain growth — a broader survey is presented here. For some compositions and phases, grain growth was not observed at all. In the Fe-rich region, for example, the σ-FeCr and fcc phases transform to bcc at the lowest annealing temperature of 200 °C. The small quantities of the α-Mn phase which remain after annealing at 200 and 400 °C cannot be considered as representative of the material — most if it has transformed to bcc as well. For the other compositions and phases, grain growth occurs too abruptly for a meaningful analysis of growth rate. Increased grain size for σ-FeCr, for example, was measured at a single temperature of 600 °C; at 800 °C the grain size was too large to measure due to limited instrumental resolution. In future work, growth rates and activation energies may be measured for a reduced number of compositions. With a data collection time of 3 s/composition, an in situ annealing study could measure a diffraction pattern from each of 200 compositions every 10 min.

5. Conclusion

Cr–Fe–Ni cosputtered films grow with grain sizes of ~7–15 nm in multiphase regions of the phase diagram;

grain sizes of >30 nm are observed where the films are nearly single phase. The phase diagram for as-deposited films is far from equilibrium, including a nonequilibrium α-Mn phase. On annealing, the α-Mn phase disappears at 200–600 °C; a general evolution from σ-FeCr to bcc to fcc is observed in the phase fields of the ternary sections. Substantial grain growth is observed in the bcc phase at 200 °C, while the fcc and σ-FeCr phases grow significantly only at 600 °C.

Acknowledgements

We are grateful for helpful discussions with I. Kosacki.

Research sponsored by the Office of Energy Efficiency and Renewable Energy, Industrial Technologies Program, Industrial Materials for the Future, under grant number DE-FC07-02ID14251, and by the Division of Materials Sciences and Engineering, U. S. Department of Energy under Contract DE-AC05-00OR22725 with UT-Battelle, LLC. The UNICAT facility at the Advanced Photon Source (APS) is supported by the Univ of Illinois at Urbana-Champaign, Materials Research Laboratory (U.S. DOE, the State of Illinois-IBHE-HECA, and the NSF), the Oak Ridge National Laboratory (U.S. DOE under contract with UT-Battelle LLC), the National Institute of Standards and Technology (U.S. Department of Commerce) and UOP LLC. The APS is supported by the U.S. DOE, Basic Energy Sciences, Office of Science under contract No. W-31-109-ENG-38.

References

[1] C. Cheung, G. Palumbo, U. Erb, Scr. Metall. Mater. 31 (1994) 735.
[2] C. Cheung, F. Djuanda, U. Erb, G. Palumbo, Nanostruct. Mater. 5 (1995) 513.
[3] H.Q. Li, F. Ebrahimi, Acta Mater. 51 (2003) 3905.
[4] M. Thuvander, M. Abraham, A. Cerezo, G.D.W. Smith, Mater. Sci. Technol. 17 (2001) 961.
[5] U. Klement, U. Erb, A.M. El-Sherik, K.T. Aust, Mater. Sci. Eng., A Struct. Mater.: Prop. Microstruct. Process. A203 (1995) 177.
[6] Y.-Y. Chuang, Y.Y. Chang, Metall. Trans., A, Phys. Metall. Mater. Sci. 18 (1987) 733.
[7] J.A. Oberteuffer, J.A. Ibers, Acta Crystallogr., Sect. B: Struct. Sci. 26 (1970) 1499.
[8] M.C. Simmonds, R.C. Newman, S. Fujimoto, J.S. Colligon, Thin Solid Films 279 (1996) 4.
[9] H. Wang, Q. Liu, J. Zhang, T.Y. Hsu, X. Zuyao, Nanotechnology 14 (2003) 696.
[10] E.D. Specht, P.D. Rack, A. Rar, G.M. Pharr, E.P. George, H. Hong, in: R.A. Potyrailo, A. Karim, Q. Wang, T. Chikyow (Eds.), Combinatorial and Artificial Intelligence Methods in Materials Science II, vol. 804, Materials Research Society, Warrendale, PA, 2003, p. 45.
[11] A. Rar, E.D. Specht, E.P. George, M.L. Santella, G.M. Pharr, J. Vac. Sci. Technol., A, Vac. Surf. Films 22 (2004) 1788.
[12] E.D. Specht, A. Rar, G.M. Pharr, E.P. George, P. Zschack, H. Hong, J. Ilavsky, J. Mater. Res. 18 (2003) 2522.
[13] B.E. Warren, X-Ray Diffraction, Dover Publications, New York, NY, 1990, p. 253.
[14] C.C. Koch, J. Narayan, in: D. Farkas, H. Kung, M. Mayo, H. Van Swygenhoven, J. Weerman (Eds.), Structure and Mechanical Properties of Nanophase Materials—Theory and Computer Simulation vs. Experiment, vol. 634, Materials Research Society, Warrendale, PA, 2001, p. B5.1.1.
[15] F.E.W. Wetmore, D.J. LeRoy, Principles of Phase Equilibria, McGraw-Hill, New York, 1951, p. 10.